IEEE Photonics Journal
An IEEE Photonics Society Publication

Open Access

Spatially Arrayed Long Period Gratings in Multicore Fiber by Programmable Electrical Arc Discharge

Volume 9, Number 1, February 2017

Ruoxu Wang
Ming Tang
Songnian Fu
Zhenhua Feng
Weijun Tong
Deming Liu

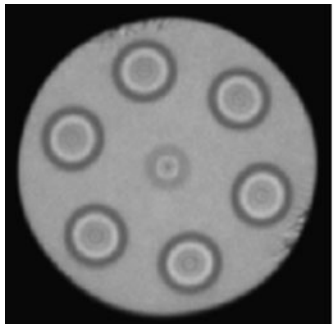

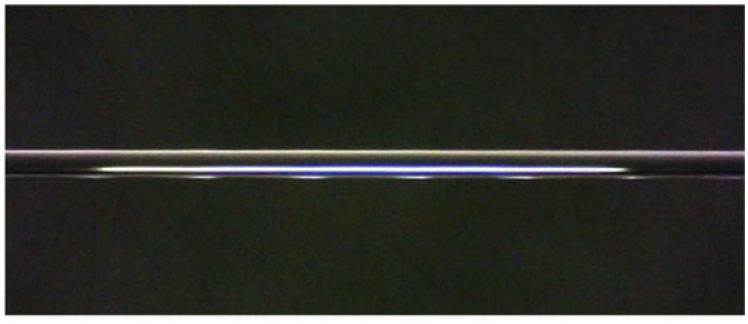

DOI: 10.1109/JPHOT.2016.2639499
1943-0655 © 2016 IEEE

IEEE photonics SOCIETY

IEEE

Spatially Arrayed Long Period Gratings in Multicore Fiber by Programmable Electrical Arc Discharge

Ruoxu Wang,[1] Ming Tang,[1] Songnian Fu,[1] Zhenhua Feng,[1] Weijun Tong,[2] and Deming Liu[1]

[1]Wuhan National Lab for Optoelectronics (WNLO) and National Engineering Laboratory for Next Generation Internet Access System, School of Optical and Electronic Information, Huazhong University of Science and Technology, Wuhan 430074, China
[2]State Key Laboratory of Optical Fiber and Cable Manufacture Technology, Yangtze Optical Fiber and Cable Joint Stock Limited Company (YOFC) R&D Center, Wuhan 430073, China

DOI:10.1109/JPHOT.2016.2639499
1943-0655 © 2016 IEEE. Translations and content mining are permitted for academic research only. Personal use is also permitted, but republication/redistribution requires IEEE permission. See http://www.ieee.org/publications_standards/publications/rights/index.html for more information.

Manuscript received November 10, 2016; revised November 29, 2016; accepted December 11, 2016. Date of publication December 16, 2016; date of current version January 4, 2017. This work was supported in part by the National Natural Science Foundation of China under Grant 61331010 and Grant 61205063 and in part by the Program for New Century Excellent Talents in University (NCET-13-0235). Corresponding author: M. Tang (e-mail: tangming@mail.hust.edu.cn).

Abstract: Based on electrical arc discharges mechanisms, we inscribed spatially arrayed long period gratings (LPGs) into a heterogeneous seven-core fiber. The LPG fabrication platform was built upon the commercial fiber fusion splicer with a self-developed real-time control software. With the help of homemade fan-in/fan-out multiplexer, the high-quality grating spectra in seven cores are measured. The largest resonant dip of −42 dB and minimum insertion loss of 0.5 dB are achieved in the central core. To demonstrate potentials of the spatially diversified gratings, we measured the strain and temperature simultaneously with the spatial response matrix to eliminate the cross sensitivity. Accurate sensing results have been achieved with relative errors less than 4%.

Index Terms: Multicore fiber, fiber grating, spatial division multiplex.

1. Introduction

As a promising solution to further extend the optical fiber communication capacity and fiber application diversity, spatial-division multiplexing (SDM) technology employing few mode fibers (FMFs) or multicore fibers (MCFs) is developing rapidly [1]. To facilitate practical SDM system exploitation, several MCF based optical devices/sub-systems are being developed by taking the advantage of spatial density, such as the erbium-doped multicore fiber amplifier [2], fiber Bragg grating in multicore fiber for curvature measurement in two axis [3], [4], long period grating in MCF as a vector bending sensor [5], and Mach-Zehnder interferometer in seven-core fiber for temperature and strain sensing [6], etc.

Long period grating (LPG) is a classical optical fiber device in optical communication and sensing fields [7]. There are various fabrication methods to inscribe LPG into the conventional and specialty fiber: UV laser exposure through the amplitude mask [8], CO_2 or femtosecond laser direct point-to-point irradiation [9], the electric arc discharges (EADs) method [10], mechanical microbends and chemical etches [11], etc. Nevertheless, most light-based methods need sophisticated

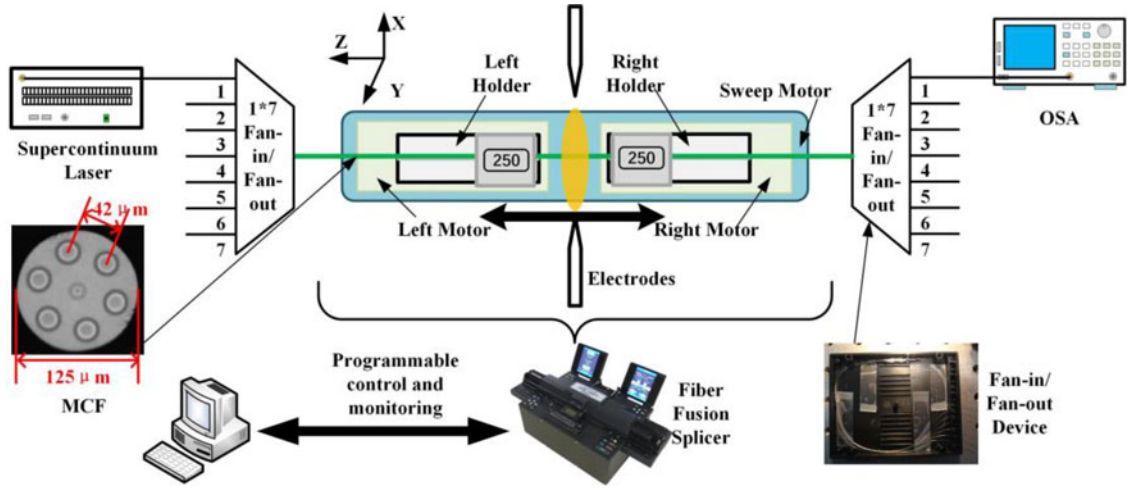

Fig. 1. Setup of the long period grating fabrication and monitoring platform in multicore fiber.

fabrication platform and pretreatment procedures like high power laser system at specific wavelength, amplitude or phase masks, and long-time hydrogen loading. For the multicore fiber, the core shadows experienced by laser pulses would decrease the grating quality and reduce the uniformity in different cores [12]. As a result, the EADs based LPG fabrication technique attracts more attention due to its simplicity and applicability for any types of fiber. In previous investigations [13], we utilized the EADs method to generate cascaded periodic micro-tapers along MCF thus the LPG can be obtained. However, multiple-micro-taper structure caused significant physical deformations of the MCF. The reduced core-to-core pitch and core diameter led to the leakage of optical field in each core and enhanced crosstalk among cores. Therefore, large transmission losses of the LPGs in parallel cores are observed, especially in the outer cores. To reduce the losses and improve the LPG quality, an advanced EADs method with refractive index modulation is thriving recently [14]–[16], which can remarkably improve the reproducibility and physical robustness of LPGs.

In this paper, based on EADs method, we developed a computer-controlled platform on top of the commercialized fiber fusion splicer to achieve high precision LPG fabrication. A spatially integrated high quality LPG array has been successfully inscribed in heterogeneous multicore fiber simultaneously with 10 nm precision of grating pitch. The transmission spectra of LPGs in different cores are measured with the spatial fan-in/fan-out multiplexer and the wavelength of the main resonant dip can be controlled from 1410 nm to 1650 nm corresponding to different grating pitches. A proof-of-concept experiment is conducted using the spatial diversified LPGs in MCF and independent measurements of temperature and strain are demonstrated. The strain/temperature spatial response matrix of LPGs in two cores has been formed and calibrated to discriminate the dual-parameter correlation effects.

2. Fabrication of LPG Array in Multicore Fiber

Fig. 1 shows the LPG fabrication and monitoring platform. A commercial fiber fusion splicer (Fujikura FSM 100P+) is applied to perform EADs. Calling the application program interface (API) of the splicer, we used C# language to develop a computer software to control the fabrication parameter, monitor the arc discharge processes and fiber conditions in real-time. In the software panels, as Fig. 2 shows, we can configure the arc discharge power, discharge time, grating periodicity number and grating pitch with the precision of 10 nm. With a pair of fan-in/fan-out multiplexer, a supercontinuum laser source as an ultra-wideband optical source (YSL Photonics SC-5-FC) from 600–1700 nm and an optical spectrum analyzer (OSA, Yokogawa AQ6370C) are used to measure

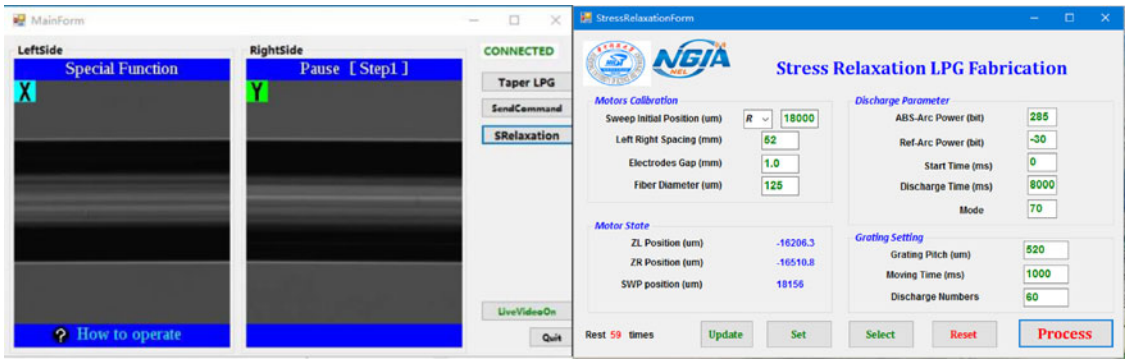

Fig. 2. Real-time control and monitoring software panels.

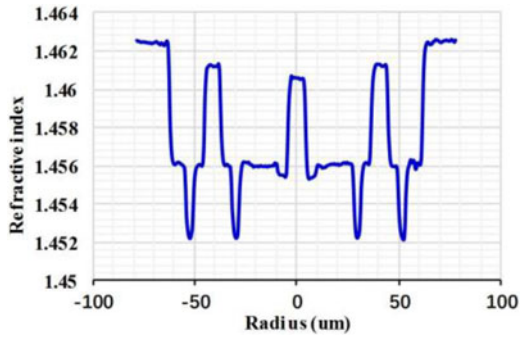

Fig. 3. Refractive index profile of the heterogeneous MCF.

the LPG transmission spectrum evolution during the fabrication. We designed and fabricated the seven-core fiber for the grating inscription and the cross section is shown in the insert of Fig. 1. The cladding diameter is 125 μm and the core pitch is 42 μm. The center core is designed with G.652 refractive index profile, the outer cores comply with the G.657.B3 standard with deep Fluorine-doped trenches as Fig. 3 shows. The average refractive indexes of cladding, central core, outer core and outer trench are 1.4560, 1.4626, 1.4636, and 1.4506, respectively. The detailed fabrication procedures of the MCF-LPG are explained as follows: 1) cleaving two separated MCF segments and putting them into the left and right fiber holders; 2) using the side-view method to fusion splice two fiber segments, while aligning left/right motors to eliminate the undesirable stress of X/Y axis [17]; 3) arc discharges with 285 bits (about 16.2 mA) and 8 seconds duration, the arc discharge-induced high-temperature heating causes residual stress relaxation and thermal diffusion of the dopant [14], [18], [19]. As a consequence, the refractive indexes in the core and cladding in each cores at the heating region are modified [14]; 4) moving the sweep motor which takes the whole MCF to the next discharge position, the moving distance determines the grating pitch Λ of the LPG; 5) repeating step 3) and 4) N times to induce periodic refractive index modulation and form the LPG in every cores of the MCF. Fig. 4(a) shows the LPG transmission spectrum evolutions in the center core of the MCF along with the grating periodicity N when the grating pitch Λ equals to 490 μm. It clearly shows with periodicity N increasing, the main resonant dip grows accordingly and approaches to a suppression ratio of 25 dB at N $=$ 50. The resonant wavelength is located at 1478.4 nm with the insertion loss of less than 0.5 dB, and the LPG total length is 24.5 mm. The microscopic photograph of the MCF-LPG with 490 μm pitch shows in Fig. 4(b).

We fabricated several groups of LPG arrays with different grating pitches from 470 μm to 530 μm, and measured the transmission spectra in the center cores of those samples as show in Fig. 5(a). The largest attenuation dip of $-$42 dB suppression ratio in the center core is achieved, as the 510 μm curve shows. The relationship between the resonant wavelength and grating pitch

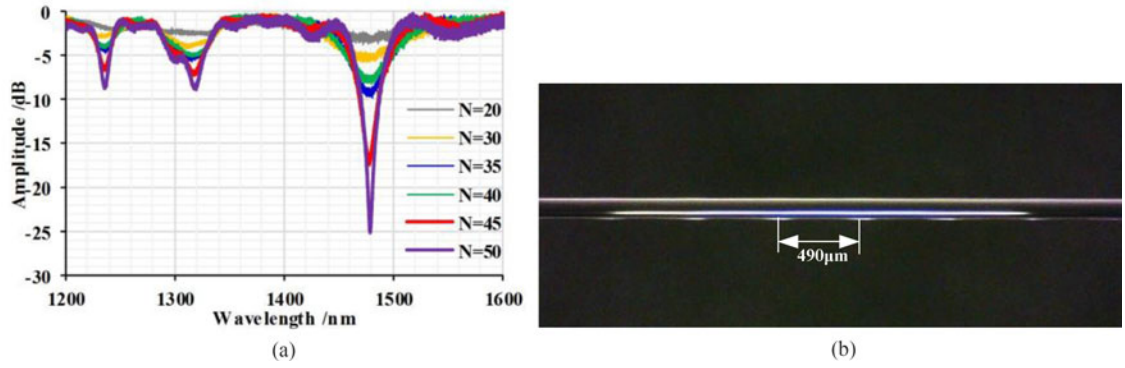

Fig. 4. (a) Transmission spectrum evolutions along with N, where the grating pitch is 490 μm. (b) Microscopic photograph of LPG inscribed in multicore fiber.

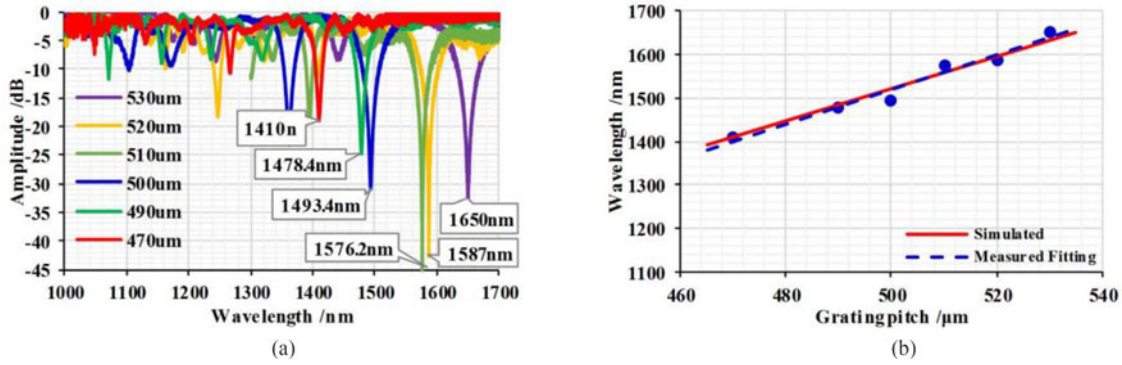

Fig. 5. (a) Transmission spectra of LPGs in the center cores of MCF with different grating pitches from 470 μm to 530 μm. (b) Relationship between the resonant dip wavelength and grating pitch, where the blue points are measured results, the blue dashed curve is the data fitting line, and the red solid line is the predicted phase matching curve according to the FEM simulation results.

is indicated in Fig. 5(b). The main resonant wavelength from 1410 nm to 1650 nm increases with the growing grating pitch, which matches the LPG resonant equation, as (1), shown below, shows, where λ_R^m is the resonant wavelength, n_{eff}^{01} and n_{eff}^{02} represent the effective refractive indices of the fundamental guided mode and the involved cladding mode of order m, respectively [20]. According to the refractive index profile in Fig. 3, we use finite element method (FEM) with COMSOL 5.0 to simulate the fundamental mode and low order cladding mode field in the central core as Fig. 6 shows, the effective refractive indexes of the two modes are 1.4597 and 1.4560 with difference of 0.0037. Then we used the FEM simulation results to predict the phase matching curve as the red line in Fig. 5(b) presented. From the slope of the measured data fitting line (blue dashed curve, 3.9 nm/μm) in Fig. 5(b) and (1), we can calculate the experimental refractive index difference Δn_{eff} of the two coupled modes is 0.0039, which is close to the simulation results. It indicates the fundamental mode and the cladding mode satisfied the phase matching condition, coupled in the forward propagating direction to generate the main notch of the LPG in the center core with different grating pitches.

$$\lambda_R^m = \Delta n_{eff} \Lambda = (n_{eff}^{01} - n_{eff}^m)\Lambda. \quad (1)$$

To investigate the LPG characteristics in different cores of the MCF, we used a pair of in-house developed customized fan-in/fan-out devices to measure the transmission spectra of the LPGs in seven cores. The spatial fan-in/fan-out pair is manufactured based on chemical etching processes and fiber bundle technique with an average end-to-end insertion loss of 3 dB per core [21], [22].

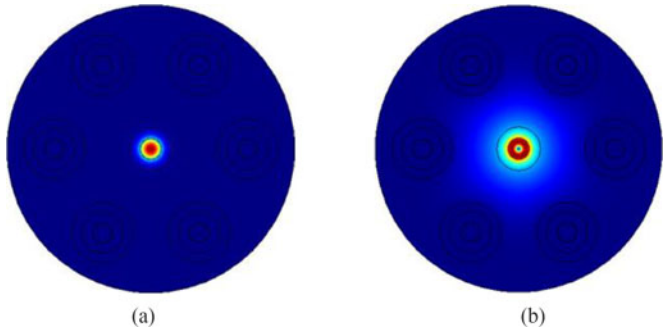

Fig. 6. (a) Simulated fundamental mode field in the center core. (b) Low order cladding mode field in the center core.

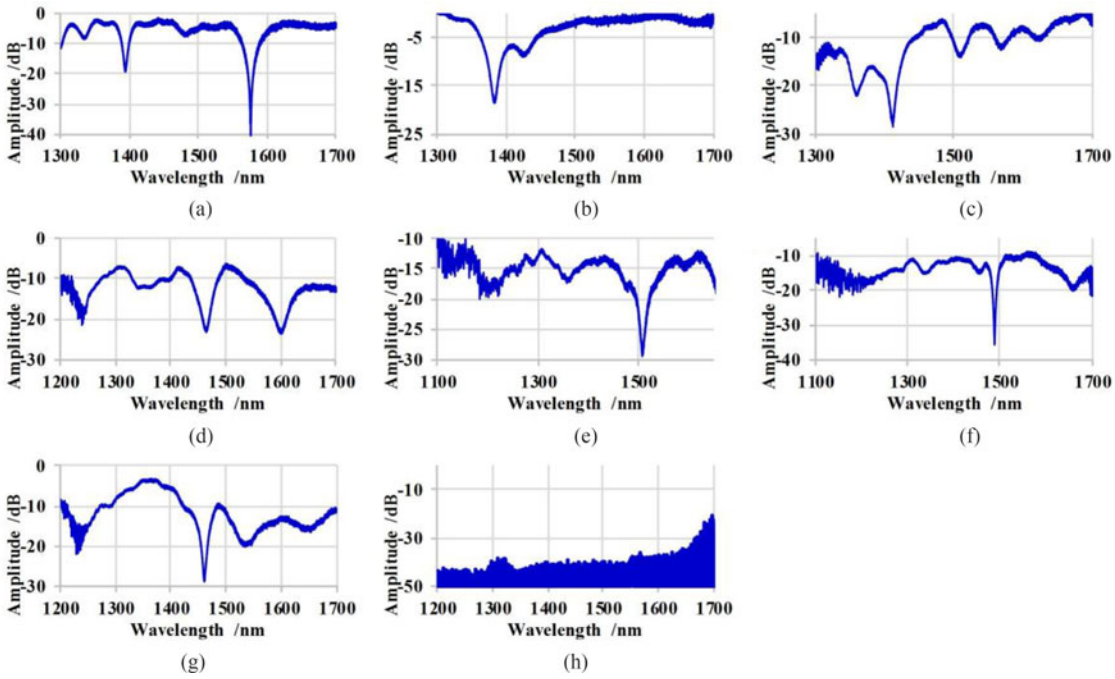

Fig. 7. Transmission spectra of LPG array in seven cores with grating pitch at 510 μm. (a) Center core transmission spectrum. (b)–(g) Outer six cores transmission spectra. (h) Crosstalk measurement when the supercontinuum light is injected into the center core and spectrum is measured in one of the outer cores.

Fig. 7(a)–(g) show LPGs' spectra in seven cores. The LPGs' main resonant dips locate at different wavelengths and the transmission losses varies from 1 to 9 dB while most of cores exhibit less than 3 dB insertion losses. The different characteristics of LPGs in different cores can be explained by the following three reasons: 1) The MCF we used is a heterogeneous fiber thus the refractive index profile of center core is different from that of outer cores; 2) the MCF is prepared and manufactured using the stack-and-draw technology [23], and thus, the residual stress in different cores is heavily dependent on the stack-and-draw process. Inevitable variations among cores are anticipated [11], [24]; 3) during the EADs processes, the exposed local MCF under two arc discharges suffered asymmetric perturbation in different part [25], [26], the temperature gradient induced dissimilar index modulation in different cores. Therefore, the resulted effective refractive index difference Δn_{eff} between core and cladding modes in different cores are diverse [14], leading to different resonant wavelengths according to (1). It is worthy to note that the large core pitch and deep trenches in

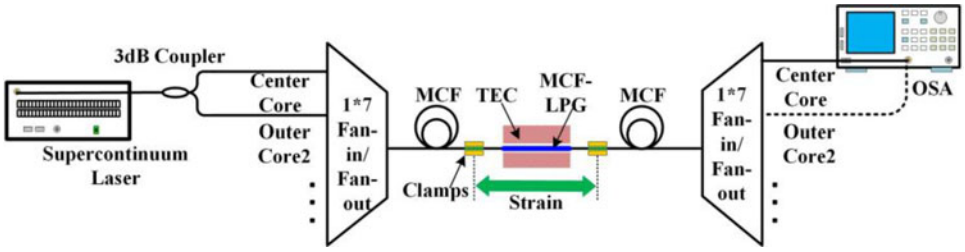

Fig. 8. Experimental setup for temperature and strain independent measurement with MCF LPG array.

the outer cores induce the sophisticated mode coupling and help to suppress the crosstalk issues among cores [6], [27], [28]. Some higher-order modes involved in the coupling and created multiple resonant dips in the transmission spectra. Fig. 7(h) illustrates the measured output spectrum from one of the outer cores when we injected the supercontinuum light into the center core. Negligible power coupling between cores can be observed thus the LPGs formed in different cores are highly independent, which is desirable for multi-parameter sensing applications.

3. Sensing Temperature and Strain with Discrimination

It is well known that temperature, strain and some other physical parameters could affect the LPG's resonant dip wavelength [7]. To demodulate the cross sensitivities and discriminate correlation effects of different parameter, many solutions have been proposed by using cascaded grating [29], [30], dual-peaks measurement [31], [32], etc. However, the cascaded structure increases the insertion losses and fabrication complexity, single physical channel also confines the numbers of the detecting parameters. Interestingly, the physically isolated paralleled LPGs proposed and achieved in the heterogeneous MCF gives us a possibility to demodulate multiple parameters eliminating cross-sensitivity by conducting spatial division multiplexing analysis. For the LPG array in MCF, the strain and temperature induced wavelength shifts $\Delta\lambda_m$ in core m can be described by (2), shown below, where $\lambda_s{}^m$ is the shifted wavelength of the LPG's main notch, $\lambda_0{}^m$ is the original wavelength of the main notch, $C\varepsilon^m$, $C_T{}^m$ are strain and temperature coefficients in core m, $\Delta\varepsilon$, ΔT are strain and temperature variations, respectively. It needs to be noted that the LPGs temperature and strain coefficients are related to the elasto-optic coefficient, thermal-optic coefficient, and the coupling modes' refractive indexes of the fiber [7], [33]. For the LPGs arrayed in the heterogeneous MCF, different cores have individually refractive index profiles and mode coupling condition as Fig. 7 implies; thus, each core has relatively dissimilar response to the temperature and strain. To eliminate the temperature and strain cross sensitivities, we selected the LPGs in center core (see Fig. 7(a)) and outer core 2 (see Fig. 7(c)) as two spatial channels. The strain and temperature responses to the wavelength shifts in different spatial channels are derived as (3) shows, where $C\varepsilon^1$ and $C_T{}^1$ represent strain and temperature coefficients in center core, $C\varepsilon^2$ and $C_T{}^2$ represent strain and temperature coefficients of LPG in outer core 2. A spatial response matrix H representing the coefficient matrix by considering two separate cores is thus defined. As long as the determinant of H det(H) is not equals to zero, the temperature and strain variations can be calculated by measuring wavelength shifts of LPGs in two cores.

$$\Delta\lambda_m = \lambda_s^m - \lambda_0^m = C_\varepsilon^m \Delta\varepsilon + C_T^m \Delta T \tag{2}$$

$$\begin{pmatrix} \Delta\varepsilon \\ \Delta T \end{pmatrix} = \begin{pmatrix} C_\varepsilon^1 & C_T^1 \\ C_\varepsilon^2 & C_T^2 \end{pmatrix}^{-1} \begin{pmatrix} \Delta\lambda_1 \\ \Delta\lambda_2 \end{pmatrix} = H^{-1} \begin{pmatrix} \Delta\lambda_1 \\ \Delta\lambda_2 \end{pmatrix} = \frac{1}{\det(H)} \begin{pmatrix} C_T^2 & -C_T^1 \\ -C_\varepsilon^2 & C_\varepsilon^1 \end{pmatrix} \begin{pmatrix} \Delta\lambda_1 \\ \Delta\lambda_2 \end{pmatrix}. \tag{3}$$

In order to determine the elements in spatial response matrix H, experiments are carried out to calibrate the strain/temperature coefficients independently, as shown Fig. 8. Both ends of the MCF-LPG are fixed at two clamps on translation stages with interval of 20 cm to induce the strain.

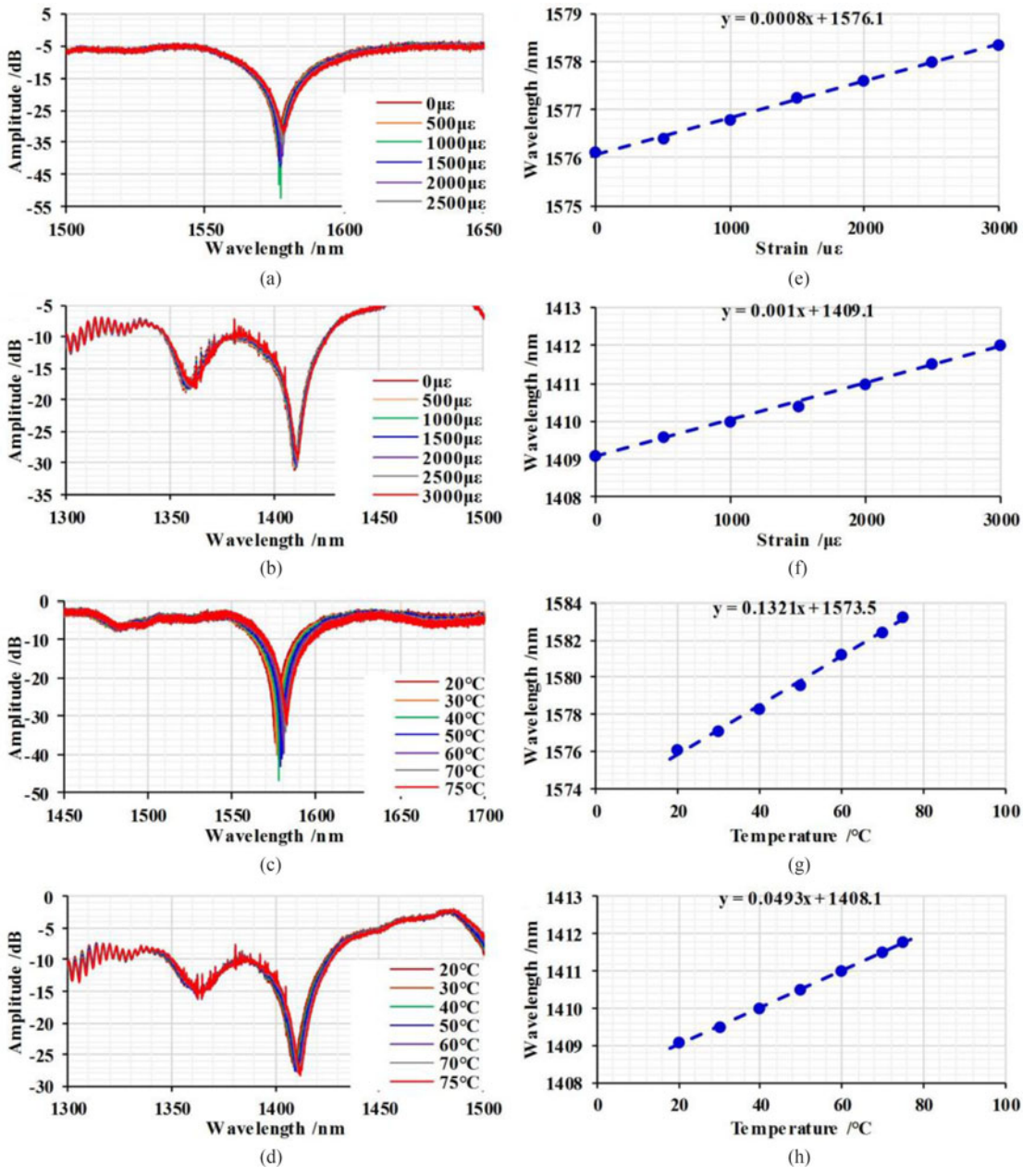

Fig. 9. (a) LPG transmission spectrum shifts in the center core with different strain at 20 °C. (b) LPG transmission spectrum shifts in outer core 2 with different strain at 20 °C. (c) LPG transmission spectrum shifts in the center core with different temperature at 0 $\mu\varepsilon$. (d) LPG transmission spectrum shifts in outer core 2 with different temperature at 0 $\mu\varepsilon$. (e)–(h) Linear fitting responses of the LPG resonant dips shifts as functions of strain/temperature variations.

The MCF-LPG is also put into a copper heater with thermoelectric cooler (TEC) to control the temperature with the resolution of 0.1 °C. Broadband light is split by a 3 dB coupler, and injected into two cores through the fan-in multiplexer. At the other end of the MCF-LPG, the spectrum shifts in different cores are spatially demultiplexed by a fan-out device and monitored by the OSA with the resolution of 0.05 nm. First, we calibrated the temperature and strain coefficients of the LPG in the center core and the outer core 2. Fig. 9(a)–(d) show the main resonant wavelength shifts of the

TABLE 1
Setting temperature and strain, measured value $\Delta\lambda 1$, $\Delta\lambda 2$, determined temperature, and strain and the relative errors

Setting parameter	Wavelength shifts		Determined parameter	Relative error [a]
	$\Delta\lambda_1$ (nm)	$\Delta\lambda_2$ (nm)		
T = 35.0 °C	2.90	1.95	T' = 34.5 °C	1.4%
S = 1200 $\mu\varepsilon$			S' = 1237 $\mu\varepsilon$	3.1%
T = 42.0 °C	4.70	3.40	T' = 41.4 °C	1.4%
S = 2300 $\mu\varepsilon$			S' = 2347 $\mu\varepsilon$	2.0%

[a] Relative error = |T'-T|/T×100% or |S'-S|/S×100%

LPG with grating pitch of 510 μm in the center core and outer core 2 when we changed the strain from 0 to 3000 $\mu\varepsilon$ at 20 °C temperature and tuned the temperature from 20 °C to 75 °C when the strain is fixed at 0 $\mu\varepsilon$. Fig. 9(e)–(h) show the linear fitting lines of resonant dip wavelength shifts versus strain/temperature variations. From the fitting lines, four elements in spatial response matrix H are obtained as follows: $C\varepsilon^1$ 0.0008 nm/$\mu\varepsilon$, $C_T{}^1$ 0.1321 nm/°C, $C\varepsilon^2$ 0.001 nm/$\mu\varepsilon$ and $C_T{}^2$ 0.0493 nm/°C. Equation (3) can then be rewritten as (4), shown below, where $\Delta\lambda_1$ and $\Delta\lambda_2$ come from (2) with the reference wavelengths $\lambda_0{}^1 = 1576.1$ nm and $\lambda_0{}^2 = 1409.1$ nm at 20 °C/0$\mu\varepsilon$ conditions, respectively.

To verify the performance of strain and temperature joint measurements with spatial response matrix, 2 experimental examples are tested and shown in Table 1. In the first case, the temperature T and strain S are set to 35 °C and 1200 $\mu\varepsilon$, respectively. The wavelengths of the resonant dip in center core and outer core 2 shift to 1579.0 nm and 1411.05 nm, respectively. Substituting the wavelength shifts $\Delta\lambda_1 = 2.90$ nm and $\Delta\lambda_2 = 1.95$ nm into (4), we can determine the measured temperature T' at 34.6 °C and strain S' at 1229 $\mu\varepsilon$, with less than 4% relative errors. Similarly, in the second case, the determined temperature and strain of 41.6 °C and 2335 $\mu\varepsilon$ are measured with the relative error less than 2%. The two measurement examples validate the effectiveness and accuracy of our SDM based MCF-LPG array in multi-parameter sensing applications.

$$\begin{pmatrix} \Delta\varepsilon \\ \Delta T \end{pmatrix} = \begin{pmatrix} -532.1 & 1425.6 \\ 10.8 & -8.6 \end{pmatrix} \begin{pmatrix} \Delta\lambda_1 \\ \Delta\lambda_2 \end{pmatrix}. \tag{4}$$

4. Conclusion

In conclusion, we successfully inscribed low-loss spatially arrayed long period gratings in heterogeneous multicore fiber based on the programmable electrodes arc discharges technology. The highly stable and precise fabrication procedures are controlled and monitored through programmable software environments. Dissimilar transmission spectra of LPGs from seven cores are obtained through a pair of fan-in/fan-out multiplexer simultaneously. A resonant dip of -42 dB and insertion loss of less than 0.5 dB in the center core has been achieved and the resonant wavelength can be tuned from 1410 nm to 1650 nm with different grating pitch. To exhibit the SDM advantages of the highly integrated LPG array, a proof-of-concept experiment is conducted to achieve a joint temperature/strain measurement with discrimination by spatial response matrix. The measurement results with relative errors less than 4% show excellent accuracy by incorporating the spatial information. Our developed

easy-to-use LPG fabrication platform is compatible with other SDM fibers, and the integrated LPG array in MCF allows us to measure more physical parameters simultaneously by building larger scale spatial response matrix with more spatial channels and high quality fan-in/fan-out devices.

Acknowledgment

The authors would like to thank Mr. Y. Li and Mr. J. Li from LUSTER LighTech Group for their technical supports of the fusion splicer.

References

[1] D. Richardson, J. Fini, and L. Nelson, "Space-division multiplexing in optical fibres," *Nature Phot.*, vol. 7, pp. 354–362, 2013.
[2] K. Abedin *et al.*, "Cladding-pumped erbium-doped multicore fiber amplifier," *Opt. Exp.*, vol. 20, pp. 20191–20200, 2012.
[3] G. Flockhart, W. MacPherson, J. Barton, J. Jones, L. Zhang, and I. Bennion, "Two-axis bend measurement with Bragg gratings in multicore optical fiber," *Opt. Lett.*, vol. 28, pp. 387–389, 2003.
[4] H. Zhang *et al.*, "Fiber Bragg gratings in heterogeneous multicore fiber for directional bending sensing," *J. Opt.*, vol. 18, 2016, Art. no. 085705.
[5] P. Saffari, T. Allsop, A. Adebayo, D. Webb, R. Haynes, and M. M. Roth, "Long period grating in multicore optical fiber: An ultra-sensitive vector bending sensor for low curvatures," *Opt. Lett.*, vol. 39, pp. 3508–3511, 2014.
[6] L. Gan *et al.*, "Spatial-division multiplexed Mach–Zehnder interferometers in heterogeneous multicore fiber for multi-parameter measurement," *IEEE Photo. J.*, vol. 8, no. 1, Feb. 2016, Art. no. 7800908.
[7] V. Bhatia and A. M. Vengsarkar, "Optical fiber long-period grating sensors," *Opt. Lett.*, vol. 21, pp. 692–694, 1996.
[8] A. M. Vengsarkar, N. S. Bergano, C. R. Davidson, J. R. Pedrazzani, J. B. Judkins, and P. J. Lemaire, "Long-period fiber-grating-based gain equalizers," *Opt. Lett.*, vol. 21, pp. 336–338, Mar. 1996.
[9] M. R. Hutsel. and T. K. Gaylord, "Residual-stress relaxation and densification in CO 2-laser-induced long-period fiber gratings," *App. Opt.*, vol. 51, pp. 6179–6187, 2012.
[10] I. K. Hwang, S. H. Yun, and B. Y. Kim, "Long-period fiber gratings based on periodic microbends," *Opt. Lett.*, vol. 24, pp. 1263–1265, Sep. 1999.
[11] Y. Wang, "Review of long period fiber gratings written by CO2 laser," *J. App. Phy.*, vol. 108, 2010, Art. no. 081101.
[12] E. Lindley *et al.*, "Demonstration of uniform multicore fiber Bragg gratings," *Opt. Exp.*, vol. 22, pp. 31575–31581, 2014.
[13] R. Wang *et al.*, "Long period grating in multicore fiber and its application for measurement of temperature and strain," in *Proc. Asia Commun. Photon. Conf.*, 2015, paper AM1D. 5.
[14] P. Wang, M. H. Jenkins, and T. K. Gaylord, "Arc-discharge effects on residual stress and refractive index in single-mode optical fibers," *App. Opt.*, vol. 55, pp. 2451–2456, 2016.
[15] G. Yin, J. Tang, C. Liao, and Y. Wang, "Automatic arc discharge technology for inscribing long period fiber gratings," *App. Opt.*, vol. 55, pp. 3873–3878, 2016.
[16] A. Iadicicco, R. Ranjan, and S. Campopiano, "Fabrication and characterization of long-period gratings in hollow core fibers by electric arc discharge," *IEEE Sens. J.*, vol. 15, no. 5, pp. 3014–3020, May 2015.
[17] K. Saito, T. Sakamoto, T. Matsui, K. Nakajima, and T. Kurashima, "Side-view based angle alignment technique for multi-core fiber," in *Proc. Opt. Fiber Commun. Conf.*, 2016, paper M3F. 3.
[18] F. Abrishamian, N. Dragomir, and K. Morishita, "Refractive index profile changes caused by arc discharge in long-period fiber gratings fabricated by a point-by-point method," *App. Opt.*, vol. 51, pp. 8271–8276, 2012.
[19] C. Colaço, P. Caldas, I. D. Villar, R. Chibante, and G. Rego, "Arc-induced long-period fiber gratings in the dispersion turning points," *J. Lightw. Tech.*, vol. 34, pp. 4584–4590, 2016.
[20] J. Estudillo-Ayala, R. Mata-Chavez, J. Hernandez-Garcia, and R. Rojas-Laguna, "Long period fiber grating produced by arc discharges," *Fib. Opt. Sen.*, vol. 1, pp. 295–316, 2012.
[21] Z. Feng *et al.*, "Multicore fiber enabled WSDM optical access network with centralized carrier delivery and RSOA based adaptive modulation," *Phot. J.*, *vol.* 7, 2015, Art. no. 7201309.
[22] B. Li *et al.*, "Experimental demonstration of large capacity WSDM optical access network with multicore fibers and advanced modulation formats," *Opt. Exp.*, vol. 23, pp. 10997–11006, 2015.
[23] A. Ziolowicz *et al.*, "Hole-assisted multicore optical fiber for next generation telecom transmission systems," *App. Phy. Lett.*, vol. 105, 2014, Art. no. 081106.
[24] C.-S. Kim, Y. Han, B. H. Lee, W.-T. Han, U.-C. Paek, and Y. Chung, "Induction of the refractive index change in B-doped optical fibers through relaxation of the mechanical stress," *Opt. Commun.*, vol. 185, pp. 337–342, 11/15/ 2000.
[25] O. Ivanov and G. Rego, "Origin of coupling to antisymmetric modes in arc-induced long-period fiber gratings," *Opt. Exp.*, vol. 15, pp. 13936–13941, 2007.
[26] S. Nam *et al.*, "Bend-insensitive ultra short long-period gratings by the electric arc method and their applications to harsh environment sensing and communication," *Opt. Exp.*, vol. 13, pp. 731–737, 2005.
[27] A. Rocha, T. Almeida, R. Nogueira, and M. Facão, "Analysis of power transfer on multicore fibers with long-period gratings," *Opt. Lett.*, vol. 40, pp. 292–295, 2015.
[28] K. Takenaga *et al.*, "Reduction of crosstalk by trench-assisted multi-core fiber," in *Proc. Opt. Fiber Commun. Conf.*, 2011, paper OWJ4.
[29] H. Patrick, G. Williams, A. Kersey, J. Pedrazzani, and A. Vengsarkar, "Hybrid fiber Bragg grating/long period fiber grating sensor for strain/temperature discrimination," *IEEE Phot. Technol. Lett.*, vol. 8, no. 9, pp. 1223–1225, Sep. 1996.

[30] L. Wang *et al.*, "Simultaneous strain and temperature measurement by cascading few-mode fiber and single-mode fiber long-period fiber gratings," *App. Opt.*, vol. 53, pp. 7045–7049, 2014.
[31] P. Caldas, G. Rego, O. V. Ivanov, and J. L. Santos, "Characterization of the response of a dual resonance of an arc-induced long-period grating to various physical parameters," *App. Opt.*, vol. 49, pp. 2994–2999, Jun. 2010.
[32] T. Geng *et al.*, "Modal interferometer using three-core fiber for simultaneous measurement strain and temperature," *IEEE Phot. J.*, vol. 8, no. 4, Aug. 2016, Art. no. 6803908.
[33] X. Shu, L. Zhang, and I. Bennion, "Sensitivity characteristics of long-period fiber gratings," *J. Lightwave Tech.*, vol. 20, 2002, Art. no. 255.